A cost-effective high-capacity OFDM based RoFSO transmission link incorporating hybrid SS-WDM-MDM of Hermite Gaussian modes

AMIT GROVER*, ANU SHEETAL
Department of Electronics and Communication Engineering, Guru Nanak Dev University, Regional Campus, Gurdaspur, India

The scarcity of RF spectrum at lower frequencies has recently been addressed by millimeter wave transmission in wireless and radio-over-free-space optics networks for more flexible frequency spectrum allocation. In this paper, we report successful transmission of 2×4×20Gbit/s-40GHz information over an orthogonal frequency division multiplexing (OFDM) based Radio-over-Free space optics (RoFSO) transmission link by incorporating hybrid spectrum-slicing based wavelength division multiplexing (SS-WDM) and mode division multiplexing (MDM) of Hermite Gaussian (HG) modes up to a link reach up to 30 km under clear weather conditions. The proposed link is also investigated under the effect of atmospheric turbulence.

(Received October 7, 2019; accepted April 9, 2020)

Keywords: SS-WDM, MDM, OFDM, RoFSO, Atmospheric turbulence

1. Introduction

The explosive increase in the need of channel bandwidth requirement as witnessed over last few decades due to rise in the use of a variety of bandwidth consuming services like social networking, video-calling, high-speed internet, live-streaming etc. have put a pressure on the limited licensed spectrum based Radio Frequency (RF) networks. Radio-over-Free space optics (RoFSO) is an important and emerging data transmission technology which shares the combined merits of both the dominant communication technologies i.e. Radio-over-fiber and free space optics links [1-3]. In RoFSO links, the costly hardware required for various information signal processing techniques like signal encoding and decoding, up- and down- frequency conversion, signal modulation and demodulation, multiplexing and de-multiplexing, handoff etc. are shared with the central base station thus reducing the overall cost and complexity of the links [4, 5]. Apart of these, other advantages are enormous capacity, large bandwidth, high-speed links, immunity to electromagnetic interference, quick and easy installation process, last-mile access, light-weight equipment, and secure links. On the other hand, orthogonal frequency division multiplexing (OFDM) is a data multiplexing technique where mutually orthogonal sub-carriers which have been divided at precise frequency interval in frequency domain are utilized to transmit high-speed data [6]. Inverse Fast Fourier Transformation algorithm is applied at the transmitter terminal to attain orthogonality. The orthogonality of the sub-carriers promises the interception of the information signal by concerned receiver unit only. The hybridization of OFDM technique with RoFSO links provides the following merits (a) high-speed links (b) mitigation of inter-symbol interference (c) high spectral efficiency (d) enhanced signal-to-noise (SNR) ratio (e) ability to deal with multipath fading and (f) mitigation of interference from co-channels [7, 8]. The authors in [9] have reported simulative development and numerical analysis of OFDM technique based RoFSO transmission link using different modulation formats under clear weather conditions. The ramifications of adverse environmental conditions on RoFSO link performance integrating OFDM technique is discussed in [10]. Further, the maximization of link transmission capabilities by multiplexing in phase dimension [11], polarization dimension [12], intensity dimension [13], code dimension [14], and wavelength dimension [15], have been reported by many researchers. Spectrum slicing based wavelength division multiplexing (SS-WDM) is a cost-effective and promising alternative to multiple coherent lasers based WDM system to facilitate multiple end users. It is capable of providing high-bandwidth scalable networks without the need for optical-electrical-optical signal processing. The authors in [16] have exploited amplified spontaneous emission for spectrum slicing in a semiconductor optical amplifier whereas spectrum slicing using arrayed waveguide grating structure is discussed in [17], and using super-luminescent diodes in [18]. The modeling and simulative analysis of SS-WDM technique in a FSO link under the effect of different environmental factors and the height of the buildings is reported in [19]. The performance comparison of different amplifiers in SS-WDM based FSO link is reported in [20]. The application of mode division multiplexing (MDM) for enhancing the capacity of RoFSO link is discussed in [21-35]. In

previously reported works [21-35], the authors have reported the use of MDM in a single wavelength channel based RoFSO link. In this article, we have demonstrated the integration of OFDM technique along with SS-WDM and MDM technique to attain 160Gbit/s-320GHz transmission. Section II describes the system modeling. Section III discusses numerical results. The conclusions are discussed in Section IV.

2. System design and parameters

The schematic diagram explaining the principle of the proposed RoFSO link is shown in Fig. 1 (a) and (b). In this work, we have used commercially available software Optisystem [36] to develop and investigate the proposed RoFSO link.

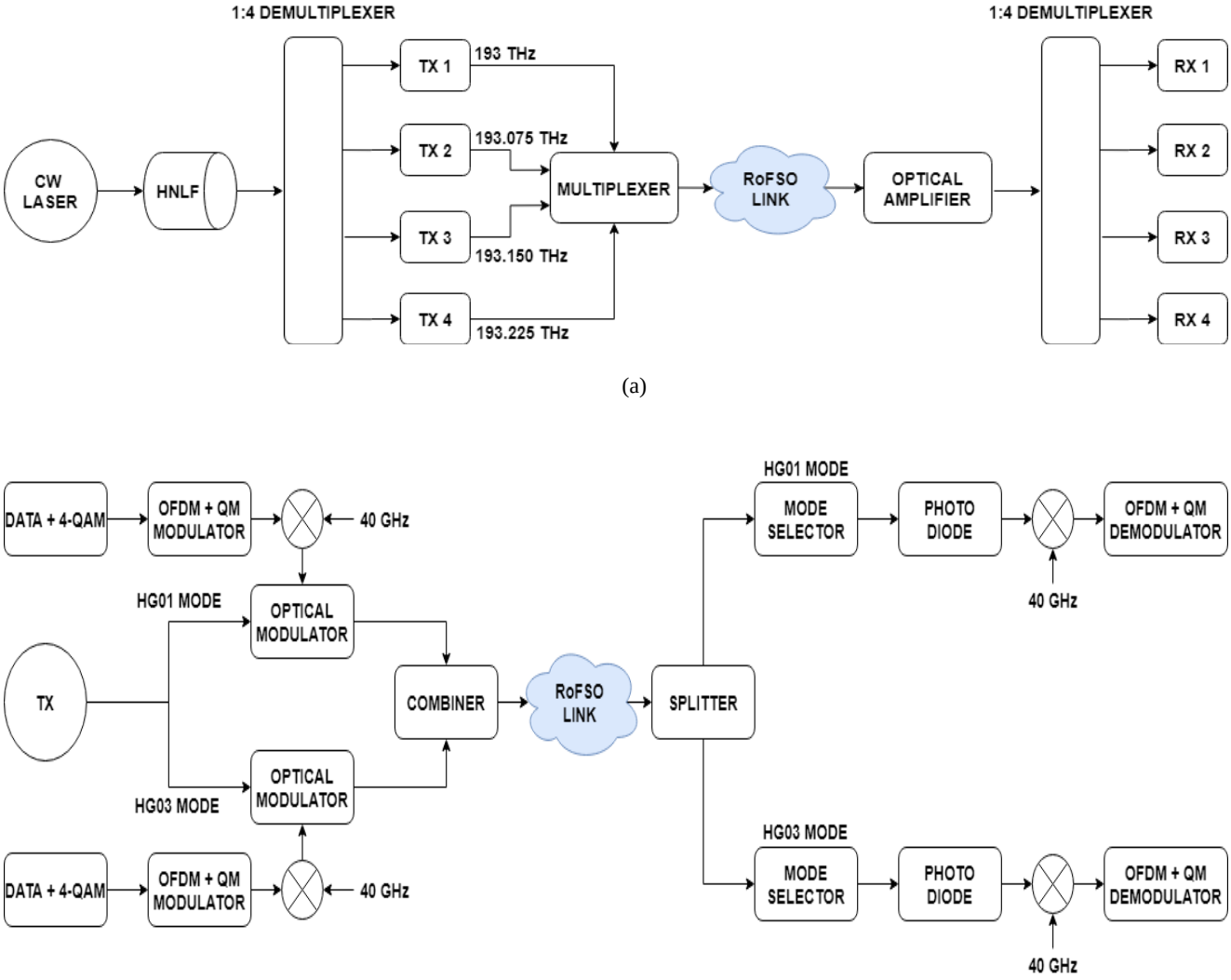

Fig. 1. (a) Schematic for the proposed super-continuum-based SS-WDM- RoFSO transmission link with four channels (b) Schematic for MDM of each sub-channel

In this work, the simultaneous transmission of multiple information signals is attained by exploiting spectrum slicing of a single beam laser signal. In traditional WDM technique reported in previous works, cost of the system in considerably increased by utilizing multiple lasers. The main focus of this work is to produce a high-powered broad-spectrum pulse for slicing. For this, we have exploited a high nonlinearity fiber (HNLF) for generating super-continuum using self-phase modulation (SPM) phenomenon. The non-linearity proportionality constant (γ_{SPM}) in a HNLF is mathematically described as [20]:

$$\gamma_{SPM} = \frac{2\pi n^2}{\lambda A_{eff}} \quad (1)$$

where refractive index of HNLF is presented by n and HNLF effective area by A_{eff}. The high powered pulse

launched into HNLF causes change in refractive index which is mathematically described as:

$$P_{nl} = \frac{3}{4}\varepsilon_0\chi^3\left|E_o(z,t)e^{[i(\omega t-\beta z]}\right| \quad (2)$$

where electrical field as a function of time (t) and frequency (ω) is expressed as $E_o(t)$ and the electric susceptibility of HNLF is expressed as χ. The effective HNLF refractive index (n) is given as:

$$n = n_o + n_2^{'}|E_o\,(z,t)|^2 \quad (3)$$

where zero field is denoted as n_o. The non-linearity in refractive index ($n_2^{'}$) is mathematically described as:

$$n_2^{'} = R_e\left[3\frac{\chi^3}{8\eta_0}\right] \quad (4)$$

The total electric filed traveling through HNLF is mathematically described as:

$$E = E_0(z,t)e^{[i(\omega_0 t-(n_0+n_2 I(z,t)k_0 z)]} \quad (5)$$

and the instantaneous frequency ($\omega^{'}$) is mathematically described as:

$$\omega^{'} = \omega_0 - n_2 k_0 z\frac{\partial I}{\partial t} \quad (6)$$

Equation (5) and (6) mathematically describe the impact of SPM on the pulse as it propagates through HNLF. Here, it can be interpreted from equations (5) and (6) that by propagating high powered pulse through an HNLF, there are extra frequency components placed on both sides of the pulse. This leads to super-continuum generation. In the proposed study, we have generated super-continuum by directing a 30 dBm laser beam from a continuous wave (CW) laser towards the input of a HNLF having 10 μm^2 effective area as illustrated in Fig. 1(a). This high powered laser beam will cause the molecules in HNLF to vibrate which further will results in refractive index variations. This will further lead to the broadening of spectrum at the output end of HNLF which can be utilized for implementing SS-WDM. The spectrum of the optical laser beam at HNLF input terminal is shown in Fig. 2 (a). The broadened frequency spectrum at the output of HNLF after super-continuum generation is shown in Fig. 2(b). Here, we have sliced four distinct channels with frequency 193 THz (channel 1); 193.075 THz (channel 2); 193.150 THz (channel 3); and 193.225 THz (channel 4) for effective bandwidth utilization as shown in Fig. 3.

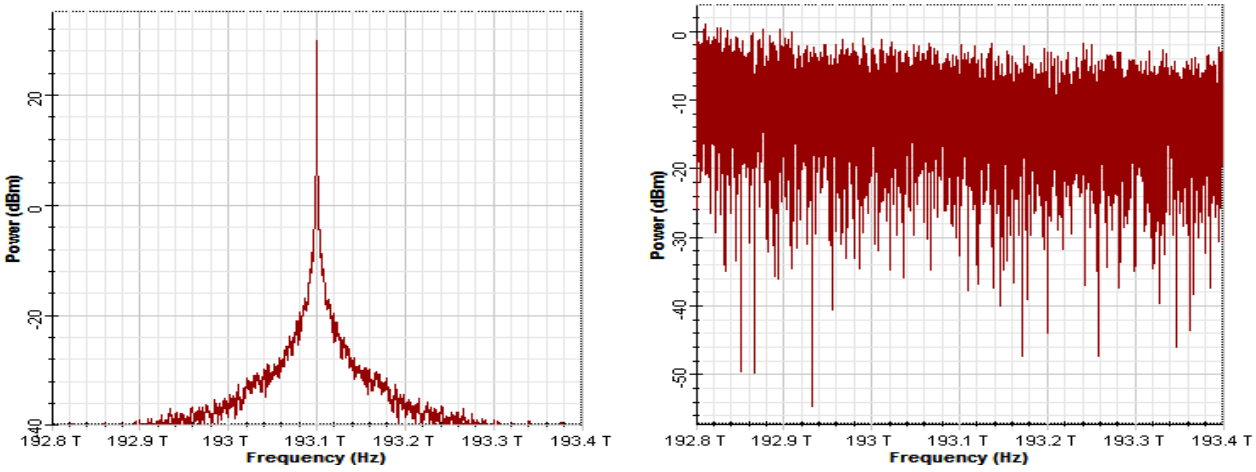

(a) (b)

Fig. 2. Optical spectrum (a) at the input of HNLF (b) at the output of HNLF after super-continuum generation

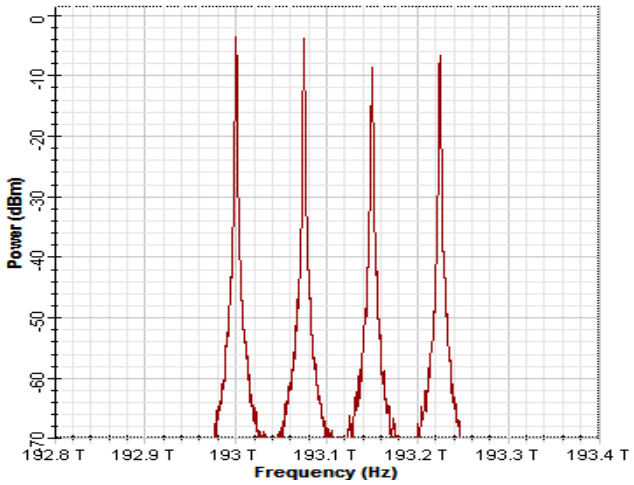

Fig. 3. Optical spectrum SS-WDM signal

For each wavelength, two independent sub-channels each carrying 20Gbit/s-40GHz are being transmitted over free space medium for varying atmospheric conditions using different HG spatial modes which are mathematically expressed as [37]:

$$\varphi_{m,n}(r,\emptyset) = H_m\left(\frac{\sqrt{2}x}{\omega_{0,x}}\right)\exp\left(-\frac{x^2}{\omega_{0x}^2}\right)\exp\left(j\frac{\pi x^2}{\lambda R_{ox}}\right)\times Hn2ywo,y\exp-y2woy2j\pi y2\lambda Roy \quad (7)$$

where dependency of modes on X-polarization and Y-polarization axis are represented by m *and* n respectively, the radius of curvature by R, the size of beam spot by w_o, and $H_m and H_n$ represents Hermite polynomials. Here, we have generated different HG modes for independent channels at the output terminal of de-multiplexer by deploying a vortex lens as illustrated in Fig. 4.

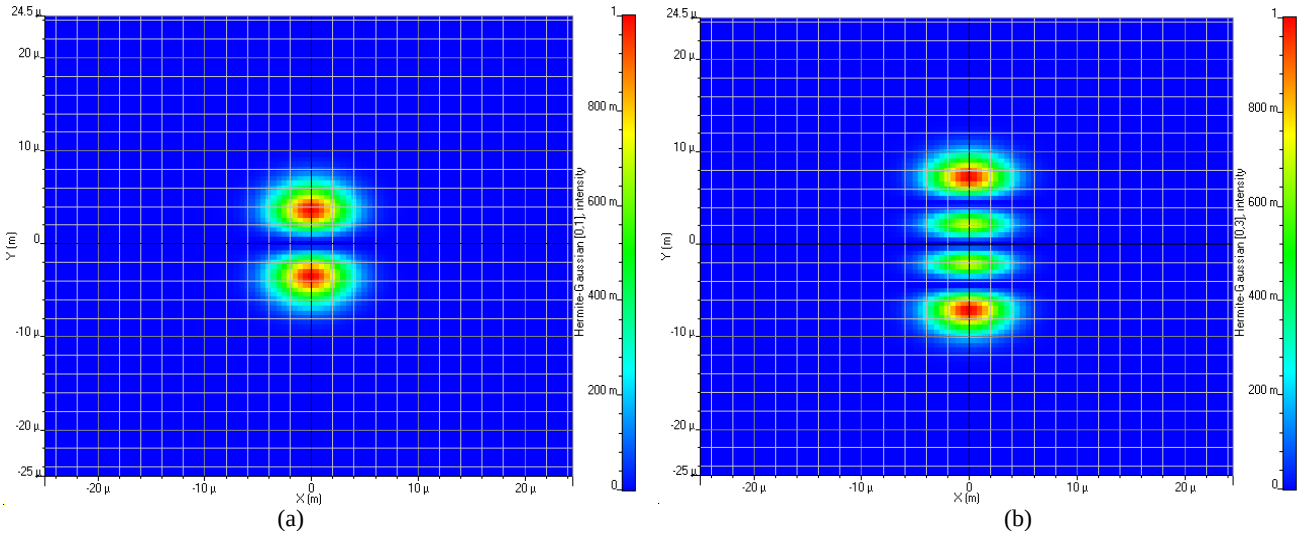

(a) (b)

Fig. 4. Excited HG modes (a) HG01 mode (b) HG03 mode (color online)

In the proposed study, we have generated 20Gbit/s information for each sub-channel by deploying a 4-Quadrature amplitude modulator (QAM). An OFDM modulator is further used where 512 subcarriers are used having 32 prefix points. 1024 IFFT algorithm is performed here. A Quadrature modulator (QM) having 15 GHz frequency is used to modulate this signal. Further, a mixer is used which adds 40 GHz RF signal to this signal. A LiNbO3 Mach-Zehnder Modulator (MZM) is deployed for modulation. The RoFSO link equation is given as [38]:

$$P_{Received} = P_{Transmitted}\left(\frac{d_R^2}{(d_T+\theta Z)^2}\right)10^{-\sigma Z/10} \quad (8)$$

where the diameter of the receiving antenna is represented as d_R, the diameter of the transmitting antenna is represented d_T, the angle of divergence of the laser beam is represented as θ, the RoFSO link range is represented as Z, and the attenuation coefficient value for different weather is represented as σ. Here, we have considered 0.25 mrad angle of divergence of laser beam, and 10 cm the diameter of receiving and transmitting antenna. The weak signal at the receiver terminal is amplified by a pre-amplifier. Different modes are separated using a mode selector component [39, 40]. A spatial PIN photo-diode converts the received optical signal from pre-amplifier to electrical signal. A QAM demodulator and OFDM demodulator are used at the demodulator section. The information signal transmitted is recovered using a QM decoder. In tropical regions like India, different fog conditions are the primary atmospheric conditions that affect the link performance. The specific attenuation due to fog can be determined using the following equation [41]:

$$\beta_{fog}(\lambda) = \frac{3.91}{V}\left(\frac{\lambda}{550}\right)^{-p} \quad (9)$$

where visibility range is represented by V (km), the wavelength of optical signal is represented by λ (nm) and scattering coefficient by p which is determined using Kim model as [42]:

$$p = \begin{cases} 1.6 & V > 50 \\ 1.3 & 6 < V < 50 \\ 0.16V + 0.34 & 1 < V < 6 \\ V - 0.5 & 0.5 < V < 1 \\ 0 & V < 0.5 \end{cases} \quad (10)$$

and Kruse model as [43]:

$$p = \begin{cases} 1.6 & V > 50 \\ 1.3 & 6 < V < 50 \\ 0.585V^{\frac{1}{3}} & V < 6 \end{cases} \quad (11)$$

Using equations (9)-(11), the attenuation coefficient for low fog condition is 9 dB/km; moderate fog is 16 dB/km; and heavy fog is 22 dB/km [26-28]. Fig. 5 discusses the geometrical losses (A_{Geo}) which are mathematically described as [44]:

$$A_{Geo} = 10log_{10}\left[\frac{4A_{RX}}{\pi(\theta Z)^2}\right]\text{dB} \quad (12)$$

where receiver surface area is represented by A_{RX}, angle of divergence of laser beam in mrad by θ, and the RoFSO link distance in km by Z

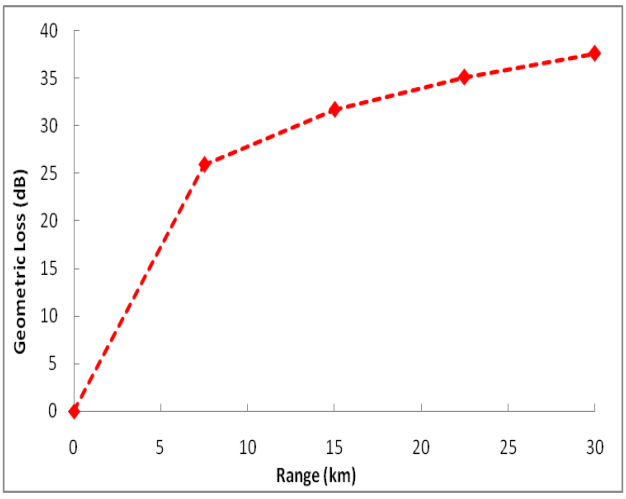

Fig. 5. Geometric loss v/s FSO link range

3. Results and discussions

Here, we present and analyze the numerical simulative investigation results of the proposed system. Fig. 6 shows the variation in signal-to-noise ratio (SNR) and optical power at the input of receiver terminal with increasing range for channel1 (193 THz) under clear weather conditions. The SNR is evaluated to be 32.84 dB, 26.78 dB, and 22.90 dB for HG01 mode and 32.07 dB, 25.55 dB, and 20.96 dB for HG03 mode at a link range of 10 km, 20 km, and 30 km respectively. Similarly, the received power is reported to be -39.38 dBm, -51.06 dBm, and -57.93 dBm for HG01 mode and -45.83 dBm, -57.47 dBm, and -64.24 dBm for HG03 mode at a link range of 10 km, 20 km, and 30 km respectively. Fig. 7 shows the constellation diagram of the received signals for channel1 at a link range of 30 km under clear weather conditions. From Fig. 7, it can be observed that the information signal received at the receiver terminal has clear constellation with unique constellation points which illustrates reliable 160Gbit/s-320GHz transmission at 30 km. The RF spectrum of the received signals for channel1 at a link range of 30 km is shown in Fig. 8. From the results, it can be observed that HG01 mode receives more RF power as compared to HG03 mode. This can be attributed to the fact that HG01 mode has more tolerance to adverse atmospheric effects. The modal decomposition of the information signals at the receiver terminal is shown in Fig. 9. For HG01 mode, the power in predominantly transferred to LP11 mode whereas rest of the power is distributed amongst LP12, LP13, and LP32 mode. Similarly, for HG03 mode, the power in predominantly transferred to LP12 whereas rest of the power is distributed amongst LP31, LP13, LP11, and LP32. The results presented agree with the spatial profiles of excited HG modes. From the results presented in Fig. 9, it can be observed that HG03 mode has higher inter-modal coupling between adjacent modes than HG01 mode. This validates the results presented in SNR and total power of received information signal plots in Fig. 6. The performance analysis of channel2 (193.075 THz), channel3 (193.150 THz), and channel4 (193.225 THz) in terms of SNR and received power are presented in Table 1.

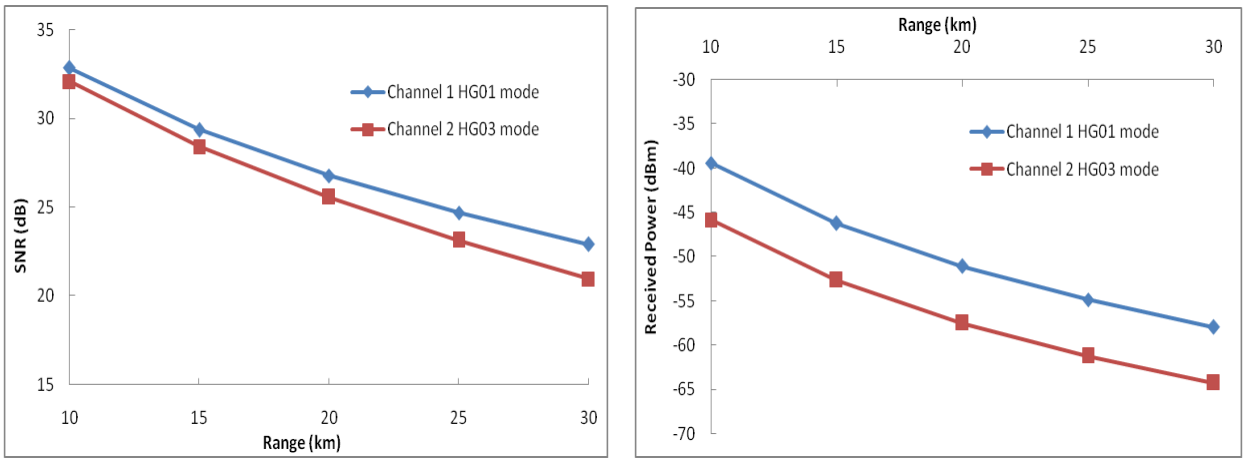

(a) (b)

Fig. 6. Measured (a) SNR (b) Received power v/s link range for channel1 (193 THz) under clear weather conditions (color online)

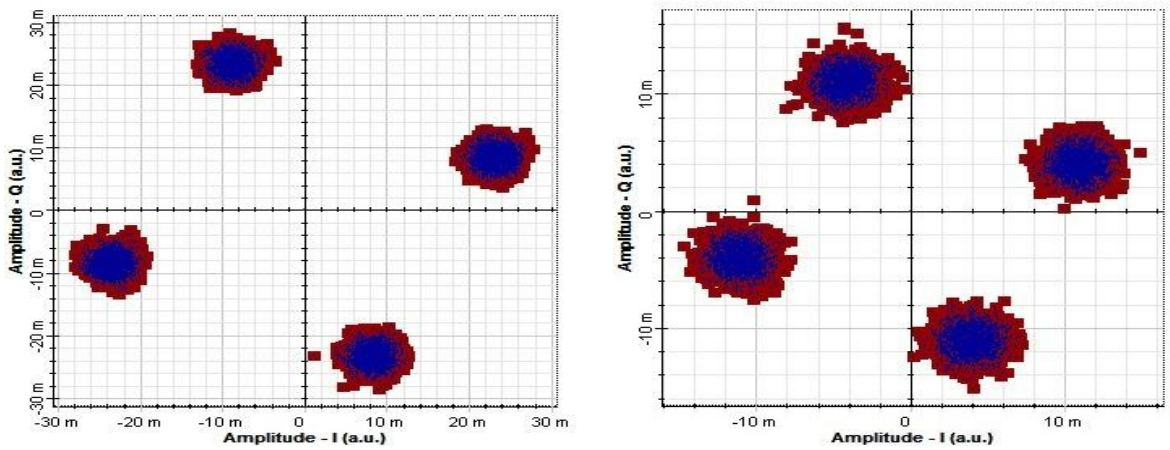

(a) (b)

Fig. 7. Constellation diagram of the received signal for channel1 (193 THz) for (a) HG01 mode (b) HG03 mode at 30 km under clear weather (color online)

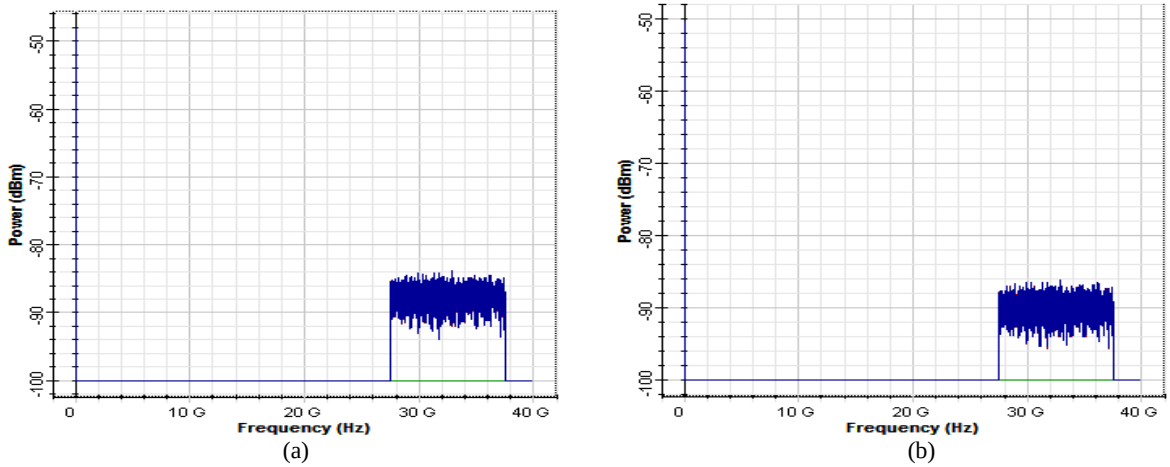

(a) (b)

Fig. 8. RF spectrum of the received signal for channel1 (193 THz) for (a) HG01 mode (b) HG03 mode at 30 km under clear weather

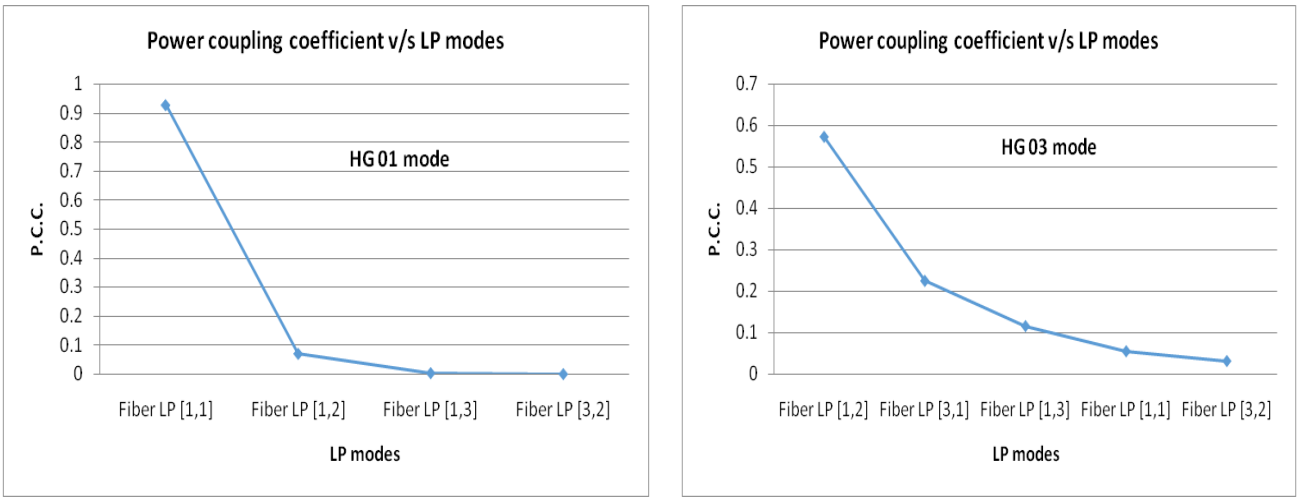

(a) (b)

Fig. 9. Modal decomposition of (a) HG01 mode (b) HG03mode at the receiver terminal

Table 1. SNR and total power of the received information signal for channel 2 (193.075 THz), channel 3 (193.150 THz), and channel 4 (193.225 THz) under clear weather conditions using the proposed link

Range (km)	**Channel 2 (193.075 THz)**				**Channel 3 (193.150 THz)**				**Channel 4 (193.225 THz)**			
	HG01		**HG03**		**HG01**		**HG03**		**HG01**		**HG03**	
	SNR (dB)	**Power (dBm)**	**SNR (dB)**	**Power (dBm)**	**SNR (dB)**	**Power (dBm)**	**SNR (dB)**	**Power (dBm)**	**SNR (dB)**	**Power (dBm)**	**SNR (dB)**	**Power (dBm)**
10	32.17	-40.12	31.66	-46.54	30.65	-42.45	29.15	-48.71	31.07	-41.85	30.77	-47.38
20	25.98	-51.83	25.02	-58.24	23.84	-54.19	22.94	-60.43	24.69	-52.16	23.86	--59.17
30	21.56	-58.75	20.93	-65.22	18.15	-60.85	17.93	-66.01	19.85	-57.49	18.12	-65.99

Also, the impact of different fog weather conditions on the proposed RoFSO link performance has been analyzed in this work. Fig. 10 analyzes the proposed link performance under the impact of varying fog weather in the terms of SNR and optical received power with increasing FSO link range. It can be observed that the SNR calculated is [40.55, 37.57, 33.53] dB, [33.38, 28.60, 21.08] dB, and [26.26, 18.04, 3.75] dB for light fog, moderate fog, and heavy fog conditions respectively at a link range of 1000 m, 1500 m, and 2000 m. Similarly, optical received power is calculated as [-29.01, -35.01,-43.00] dBm, [-43.31, -52.28,-64.08] dBm, and [-56.30, -67.92,-78.87] dBm for light fog, moderate fog, and heavy fog conditions respectively at a link range of 1000 m, 1500 m, and 2000 m. From the results presented in Fig. 10, it can be seen that the maximum FSO link range with acceptable performance (SNR~20dB) [26-28] is above 2000 m for light fog conditions which reduce to 1800 m for moderate fog and 1400 m for heavy fog conditions using the proposed link. The constellation plots and received RF power spectrum at 2000 m using the proposed link for varying level of fog conditions is illustrated in Fig. 11 and 12 respectively.

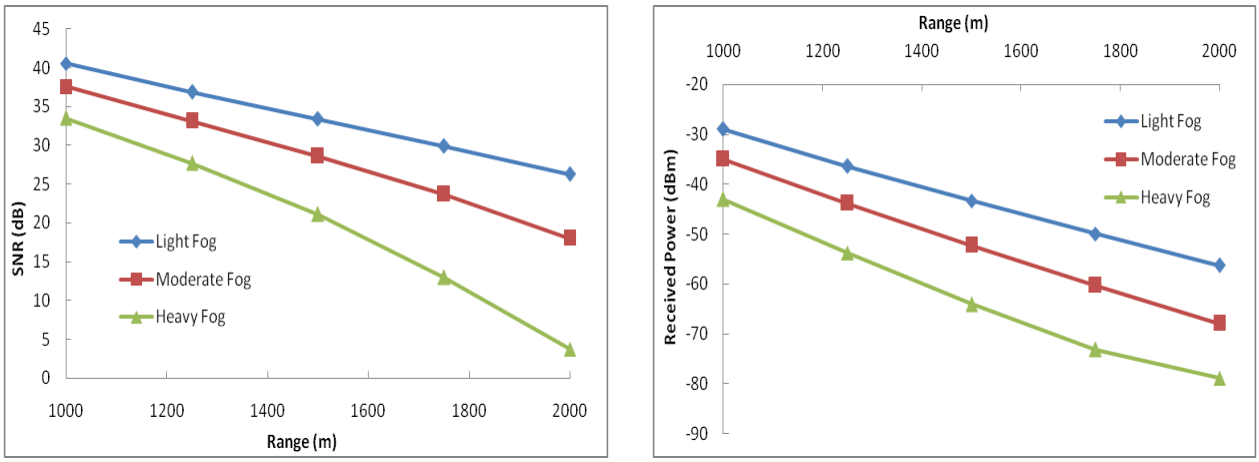

(a) (b)

Fig. 10. Measured (a) SNR (b) Received power v/s FSO link range for channel1 (HG01 mode) under different fog conditions (color online)

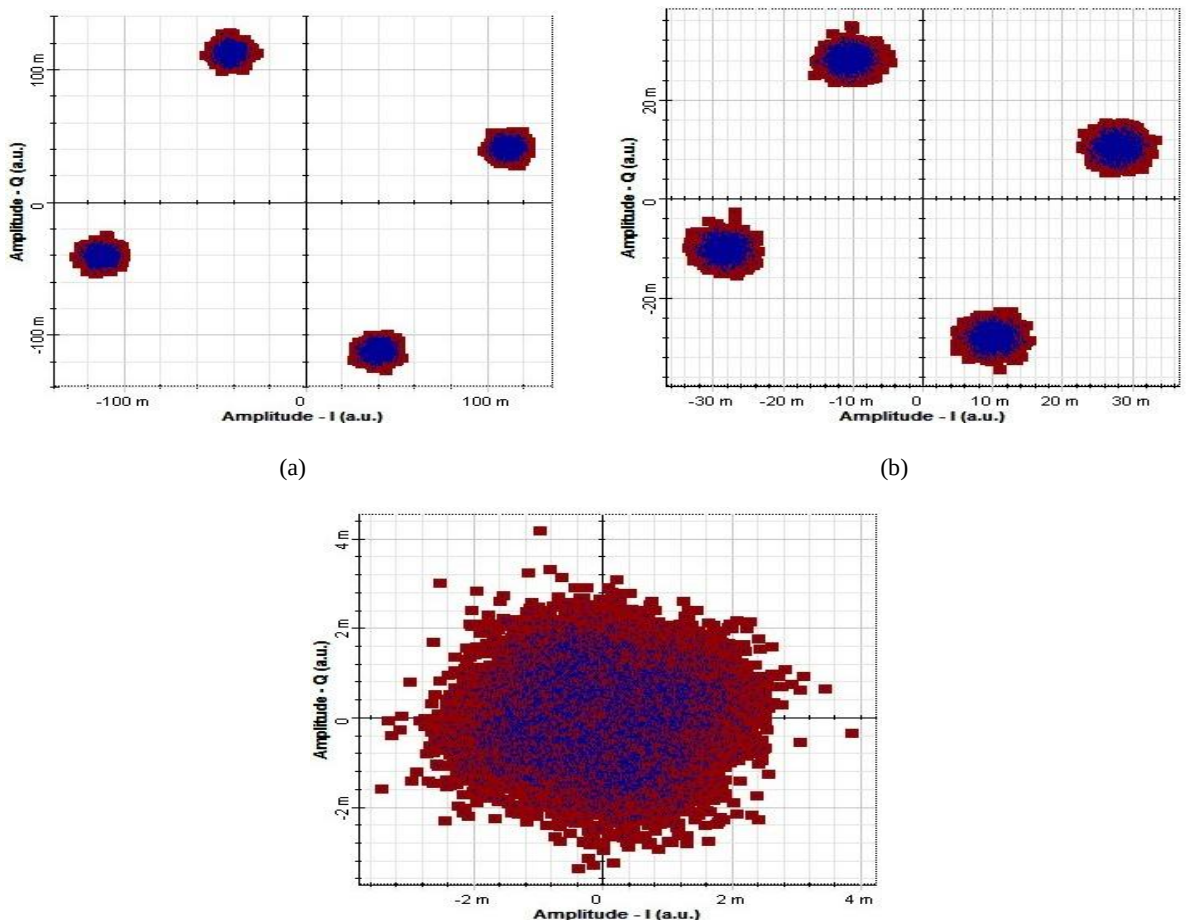

(a) (b)

(c)

Fig. 11. Constellation plots for channel 1 (HG01 mode) at 2000m under (a) Light fog (b) Moderate fog (c) Heavy fog conditions (color online)

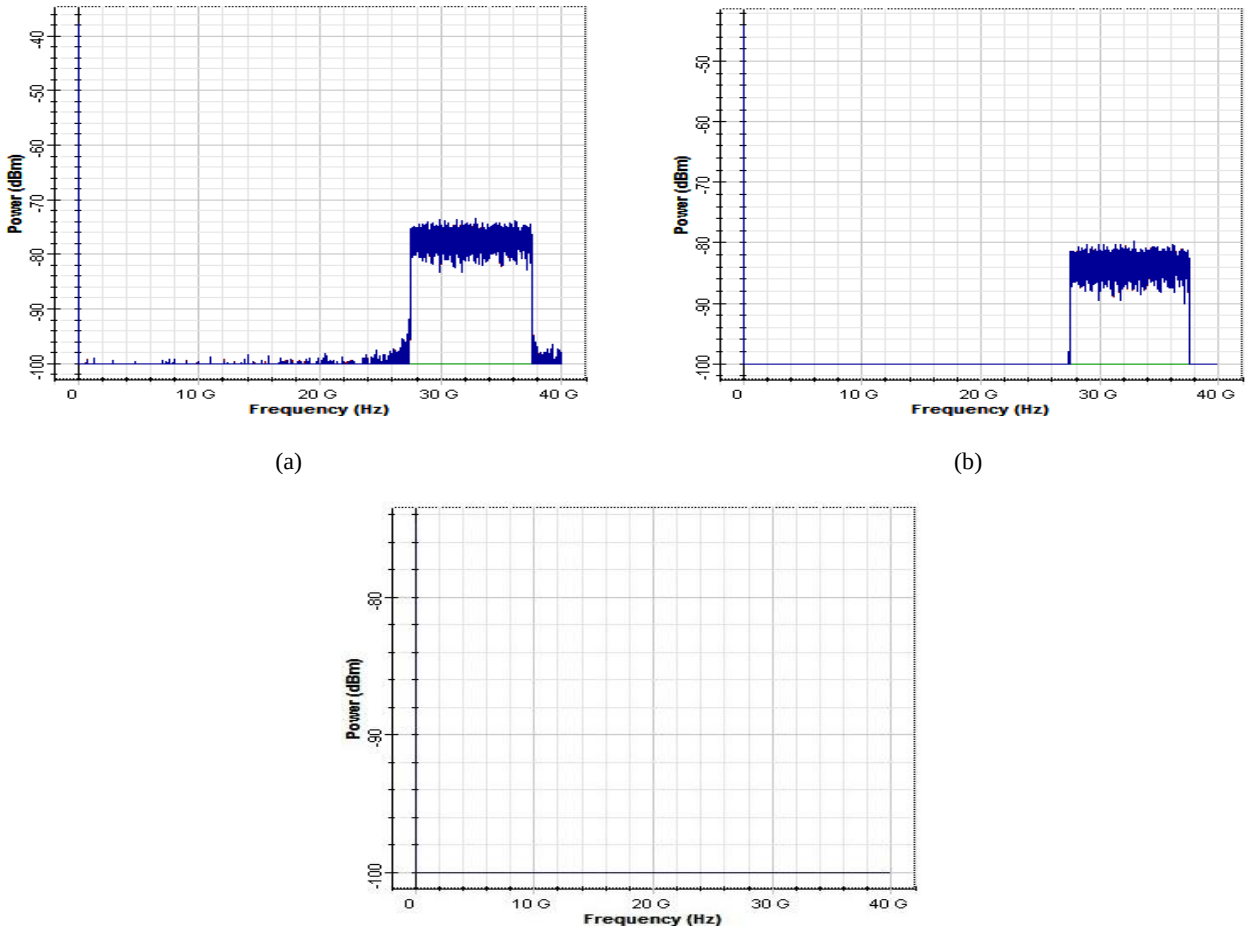

Fig. 12. RF spectrum for channel1 (HG01 mode) at 2000m under (a) Light fog (b) Moderate fog (c) Heavy fog conditions (color online)

4. Conclusions

In this work, we have reported the modeling and performance analysis of hybrid SS-WDM-MDM based OFDM RoFSO transmission link and the results have been presented that shows a successful transmission of 160Gbit/s-320GHz information over a link range of 30 km under clear weather conditions using the proposed link. The proposed link is also analyzed under the effect of atmospheric turbulence. The numerical results demonstrate that the proposed system prolongs to over 2000 m with an acceptable performance under light fog conditions which reduce to 1800m under moderate fog and 1400 m under heavy fog conditions.

References

[1] M. A. Khalighi, M. Uysal, IEEE Communications Surveys & Tutorials **16**(4), 2231 (2014).
[2] A. Mahdy, J. S. Deogun, Proceedings of IEEE Wireless Communications and Networking Conference **4**, 2399 (2004).
[3] G. Nykolak, P. F. Szajowski, G. Tourgee, H. Presby, Electronics Letters **35**(7), 578 (1999).
[4] S. A. Al-Gailani, A. B. Mohammad, R. Q. Shaddad, Proceedings of IEEE 3rd International Conference on Photonics 121 (2012).
[5] A. Ramezani, M. R. Noroozi, M. Aghababaee, International Journal of Engineering and Advanced Technology **4**(1), 46 (2014).
[6] J. Singh, N. Kumar, Optik - International Journal of Light and Electron Optics **124**(20), 4651 (2013).
[7] S. Attri, C. Narula, S. Kumar, Proc. of International Conference on Intelligent Communication, Control, and Devices **479**, 167 (2016).
[8] V. Sharma, G. Kaur, Optik - International Journal of Light and Electron Optics **124**(23), 6111 (2013).
[9] S. Chaudhary, A. Amphawan, K. Nisar, Optik–International Journal of Light and Electron Optics **125**(18), 5196 (2014).
[10] N. Kumar, A.K. Sharma, V. Kapoor, Journal of Optical Communications **35**(2), 151 (2013).
[11] C. B. Naila, K. Wakamori, M. Matsumoto, Optical Engineering **50**(10), 105006-1-9 (2011).
[12] X. Tang, Z. Ghassemlooy, S. Rajbhandari, W. O. Popoola, C. Ghiu Lee, Journal of Lightwave

Technology **30**(16), 2689 (2012).
[13] A. Kanno, K. Inagaki, I. Morohashi, T. Sakamoto, T. Kuri, I. Hosako, T. Kawanishi, Y. Yoshida, K. Kitayma Optics Express **19**(26), B56 (2011).
[14] H. Al-Khafaji, S. A. Aljunid, A. Amphawan, H. A. Fadhil, A. M. Safar, Journal of the European Optical Society-Rapid Publications **8**(13022), 13022-1-5, (2013).
[15] H. Zhou, S. Mao, P. Agrawal, Proceedings of 2014-Wireless Communications and Networking Conference (WCNC), 2677 (2014).
[16] K. Lee, S. Lim, Y. Jhon, C. Kim, P. Ghelfi, A. Nguyen, L. Poti, S. Lee, Optical Fiber Technology **18**(2), 112 (2012).
[17] F. Rashidi, J. He, L. Chen, Optics Communications **387**(68), 296(2017).
[18] G. Pendock, D Sampson, Journal of Lightwave Technology **14**, (10), 2141(1996).
[19] K. Prabhu, S. Charanya, M. Jain, D. Guha, Optics Communications **403**, 73.80 (2017).
[20] A. Thakur, S. Nagpal, Journal of Optical Communications **41**(1), 9 (2018).
[21] S. Chaudhary, A. Amphawan, International Journal of Electronics Letters **7**(3), 304 (2019).
[22] S. Chaudhary, X. Tang, X. Wei, International Journal of Electronics and Communications **93**, 208 (2018).
[23] S. Chaudhary, A. Amphawan, Photonic Network Communications **36**, 263 (2018).
[24] S. Chaudhary, A. Amphawan, Laser Physics **28**(7), 075106-1-9 (2018).
[25] S. Chaudhary, A. Amphawan, Photonic Network Communications **35**, 374 (2018).
[26] S. Chaudhary, A. Amphawan, Optical Engineering **56**(11), 116112-1-5 (2017).
[27] S. Chaudhary, A. Amphawan, International Conference on Applied Photonics and Electronics **162**, 01020-1-4 (2017).
[28] H. Srangal, A. Singh, J. Malhotra, S. Chaudhary, Optical and Quantum Electronics **49**(184), 1-10 (2017).
[29] D. Kaur, S. Chaudhary, Microwave and Optical Technology Letters **58**, 1613 (2016).
[30] A. Amphawan, S. Chaudhary, Advanced Science Letters **21**(10), (2015).
[31] M. Singh, J. Malhotra, Wireless Personal Communications **107**, 1549 (2019).
[32] M. Singh, J. Malhotra, Optical Engineering **58**(4), 046112-1-9 (2019).
[33] M. Singh, J. Malhotra, Photonic Network Communications **38**, 378 (2019).
[34] M. Singh, J. Malhotra, Wireless Personal Communications **110**, 699 (2020).
[35] M. Singh, J. Malhotra, Wireless Personal Communications **111**, 825 (2019).
[36] Optiwave, Optisystem, Ottawa, Canada, 2014.
[37] A. Ghatak, K. Thyagarajan, "An introduction to Fiber Optics", Cambridge University Press, Cambridge (1998).
[38] D. R. Kolev, K. Wakamori, M. Matsumoto, Journal of Lightwave Technology **30**(23), 3727 (2012).
[39] A. Mourka, M. Mazilu, E. Wright, K. Dholakia, Scientific Reports 3, Article No. 1422, (2013).
[40] A. Amphawan, D. O'Brien, International Conference on Photonics, 1 (2010).
[41] L. C. Andrews, R. L. Phillips, "Laser Beam Propagation Through Random Media, Second edition, SPIE Press Book, Bellingham WA, 2005.
[42] I. Kim, B. Mcarthur, E. Korevaar, Proc. of SPIE Optical Wireless Communication **6303**, 26 (2006).
[43] P. W. Kruse, L. D. McGlauchlin, R. B. McQuistan, "Elements of infrared technology: Generation, transmission, and detection", Wiley, 1962.
[44] Recommendation ITU-R, P.1814, May 2—7.

*Corresponding author: amitgrover321@gmail.com